2024 IEEE Intelligent Vehicles Symposium (IV)
June 2-5, 2024. Jeju Island, Korea

Heterogeneous Vehicle Motion Planning Considering Multiple Differentiated Characteristic Constraints

Haijie Guan, Boyang Wang, Xinping Li, Ji Li, Huiyan Chen

2024 IEEE Intelligent Vehicle Symposium (IV) | 979-8-3503-4881-1/24/$31.00 ©2024 IEEE | DOI: 10.1109/IV55156.2024.10588757

Abstract— **Revealing differences in vehicle characteristics is critical to enhancing the accessibility of heterogeneous vehicles in off-road environments. Decomposing complex motions into primitives facilitates the maintenance of the algorithm's solution efficiency while considering various constraints. Therefore, this paper proposes a heterogeneous vehicle motion planning method for off-road scenarios based on the generation, extension, and selection of driving behavior primitives. Based on the library of heterogeneous vehicle driving behavior primitives (HDBPs) extracted from driving data in our previous study, this paper proposes a primitive offline optimization generation method that integrates driving behavior constraints, vehicle kinematics constraints, reserved power constraints, and ground adhesion constraints. The generation of spatiotemporal coupled planning results is accomplished by HDBP extension and selection using the optimized HDBP library as the source. In particular, the extension and selection cost considers the interaction with the ground under the constraints of the suspension system, as well as the capacity of the drive system. This paper demonstrates that the proposed HDBP-based planning method can generate highly adaptable and differentiated primitive sequences based on diverse terrain conditions and heterogeneous vehicle characteristic constraints. Moreover, benefiting from the suspension-based pose estimation and drive system characteristic limitations, the method proposed in this paper has a significant advantage over the comparison methods in terms of terrain traversability in real-scene motion planning experiments.**

I. INTRODUCTION

Unmanned driving of heterogeneous vehicles in off-road environments has broad application scenes in disaster relief and mining area transportation [1]. Compared with a structured environment, the off-road environment contains diverse terrain semantic surface [2] and terrain geometric roughness [3]. In addition, heterogeneous vehicles with distinct steer, drive, and suspension systems behave differently in off-road environments. Heterogeneous vehicle motion planning in off-road environments needs to address two challenges. First, how to consider the constraining effect of heterogeneous vehicles' differentiated characteristics on the planning results from multiple perspectives; Second, how to evaluate the interaction between terrain features and heterogeneous vehicles in off-road scenes.

Motion planning based on primitives has the advantages of strong adaptability and high efficiency in environments without a well-defined reference [4]. In order to enhance the ability of primitives to adapt to vehicles and scenes, the researchers carried out studies on the optimal generation of primitives under certain constraints. The steering actuator constraint [5] and spatial state constraint [6] of the vehicle are considered in the generation of motion primitives. Further, the driving behavior defined by the rules and vehicle kinematic model are used as constraints to optimize the generation of primitives [7]. Furthermore, primitive generation considering human-like constraints can be accomplished by extracting primitives from the driving data [9], [17]. However, although the above methods constrain the optimal generation of primitives from multiple perspectives, they do not fully exploit the differences in the characteristics of heterogeneous vehicles under different terrain conditions.

Terrain traversability is a core element to be evaluated in a motion planning approach in the off-road environment. Some methods evaluate terrain traversability based on rules [5] or deep learning method [2], [10], [12] to guide the trajectories generation. However, the above method only assumes the vehicle as a mass point to complete the traversability calculation. To overcome the shortcomings of the vehicle mass point model in pose estimation, some methods consider the vehicle as a rigid body, use rectangular [3], [13], ellipsoid [1] to estimate the pose. Moreover, the derivative of the pose is used to evaluate the traversability of the terrain. In order to assess terrain traversability efficiently, surfels are introduced to simplify the representation of a dense point cloud [11], and several regressing costs related to the kinematic and physical constrain defined by the parameter of the surfels. However, these methods mentioned above do not consider the vehicle's suspension system. Zhang et al. [14] consider the suspension system of the vehicle when estimating the pose but do not analyze the ground contact point, which cannot handle the partial contact-free situation. Some methods guide the generation of the traversability cost by constraining the driving behavior in a specific terrain [15], [16]. However, the specificity of the terrain-behavior correspondence limits their application in general scenes. Moreover, all of the above methods ignore the consideration of vehicle drive system characteristics and do not provide an in-depth study of the differences between heterogeneous vehicles.

This paper proposes a motion planning method in an off-road environment, as shown in Fig.1, namely consisting of three main parts: Generation, Extension, and Selection of heterogeneous vehicle driving behavior primitive(HDBP). In our previous works, we developed a coordinated motion planning framework for heterogeneous vehicles [18]

This work was supported by the National Natural Science Foundation of China under Grant 52302489 and in part by the Beijing Institute of Technology Research Fund Program for Young Scholars. (Corresponding author: Boyang Wang)

All the authors are with the School of Mechanical Engineering, Beijing Institute of Technology, Beijing 100081, China. boyang_wang@bit.edu.cn

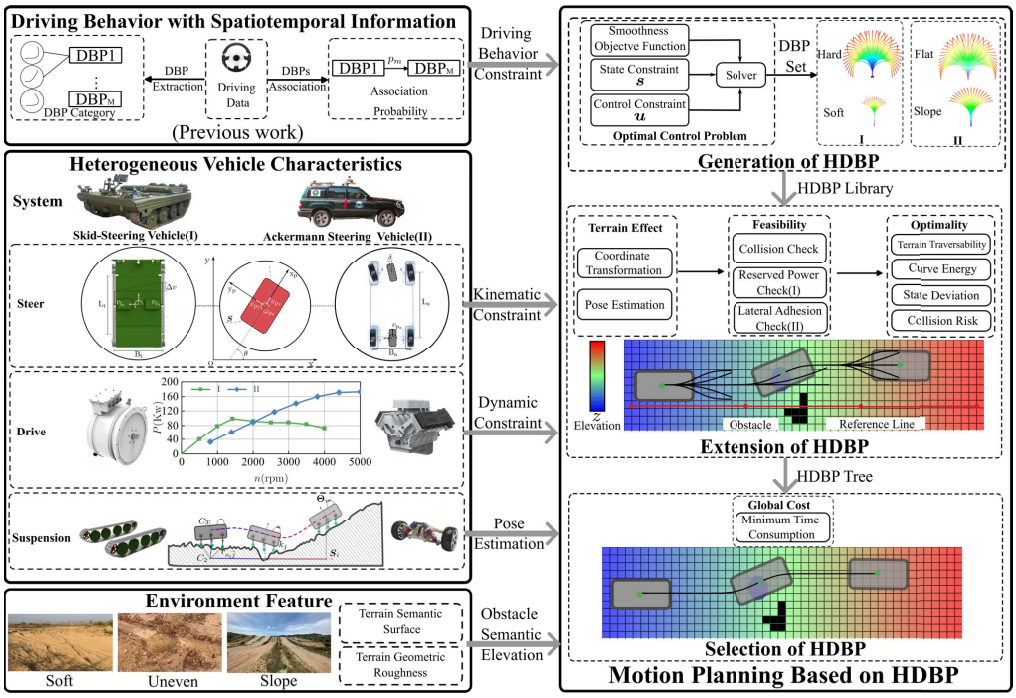

Fig. 1. Overall framework of proposed method

based on the constructed driving behavior primitive library [17]. Compared to the previous work, this paper considers more heterogeneous vehicle characteristic differentiation constraints and enhances the analysis of off-road terrain on heterogeneous vehicle traversability. Specifically, in the part of generation of HDBP, this paper adds the consideration of environmental features and heterogeneous vehicle drive system dynamics to provide more refined constraints on the control boundaries in the HDBP generation process. In the part of the extension of HDBP, the pose estimation considering the suspension system and ground contact is introduced. Based on the estimated pose, the HDBP set is further filtered by considering the drive system reserved power and lateral adhesion constraints to generate a more feasible HDBP tree for the HDBP selection.

Hence, the main contributions of the paper are as follows:

- A HDBP optimization generation method is proposed that comprehensively considers off-road environment scene elements, driving behaviors, and differences in the characteristics of heterogeneous vehicle steering, drive, and suspension systems.
- A HDBP extension and selection approach incorporating differentiated dynamics constraints for heterogeneous vehicles and suspension-based position estimation considering multi-point contacts is proposed.

II. METHODOLOGY

A. Generation of HDBP Library

The differentiated HDBP library is generated under a unified generation framework by combining the unique motion characteristics of the heterogeneous vehicles and the characteristics of different environment features. The HDBP optimization generation problem that integrates driving behavior constraints with spatiotemporal information, the kinematic model of the heterogeneous vehicle, the control boundaries of the dynamic model with the vehicle's pose and transmission structure, and the inherent longitudinal and lateral coupling laws of the vehicle itself are established as follows.

$$\begin{aligned} \min_{\boldsymbol{u}}: \quad & g_{\mathrm{s}}(\boldsymbol{s},\boldsymbol{u}) \\ s.t. \quad & \dot{\boldsymbol{s}}(t)=f_{\mathrm{d}}(\boldsymbol{s}(t),\boldsymbol{u}(t)) \qquad t\in[t_1,t_{\mathrm{g}}] \\ & \boldsymbol{s}(t)=\boldsymbol{B}_e \qquad t=t_1,\cdots,t_1+N_s\cdot\Delta t_{\mathrm{b}} \\ & (\boldsymbol{s}(t),\boldsymbol{u}(t))\in\boldsymbol{U}_{\mathrm{m}} \qquad t\in[t_1,t_{\mathrm{g}}] \\ & (\boldsymbol{s}(t),\boldsymbol{u}(t))=\boldsymbol{T} \qquad t=t_1,t_{\mathrm{g}} \end{aligned} \tag{1}$$

where $\boldsymbol{u}$ represents the control input of the heterogeneous vehicle, also serving as the optimization variable in the optimization problem, $\boldsymbol{s}$ denotes the state variables of the heterogeneous vehicle, g_{s} is the objective function composed of parameters related to trajectory smoothness, f_{d} represents the differential constraints derived from the kinematic model of the heterogeneous vehicle, relating to state and control variables, B_e represents driving behavior constraints with spatiotemporal information, $\boldsymbol{U}_{\mathrm{m}}$ represents inequality constraints derived from the dynamic model of the platform and the external characteristics of the drive system, $\boldsymbol{T}$ represents the transition constraints for the motion primitive extension process. $[t_1,t_{\mathrm{g}}]$ represents the optimization time domain, t_1, t_{g} is the start and end time of the HDBP, Δt_b represents the sampling time interval for driving behavior constraints, and N_s is the number of driving behavior constraint sampling points.

Vehicle differential constraint, driving behavior constraint, transition constraint, and the objective function are the work of the previous study [18]. This paper combines the dynamic

model of heterogeneous vehicles, and uses ground adhesion and reserved power to further expand the inequality constraints of the vehicles.

$$\begin{aligned}
F_G &= G\sin\alpha \\
\mathcal{A} &= \sqrt{1-\sin^2\alpha-\sin^2\beta} \\
x_0 &= \sigma h_{\mathrm{g}}\frac{\sin\alpha}{\mathcal{A}_{\mu_{\max}}} \\
\mu &= \frac{}{0.925+0.15R/\mathrm{B_t}} \\
F_f^{i/o} &= fG\mathcal{A}\left(\frac{1}{2}\pm\frac{h_{\mathrm{g}}\sin\beta}{\mathrm{B_t}}\right) \\
\lambda_x &= \sigma\frac{\frac{-\mathrm{L_t^2}}{6\left|x_0\right|}+\sqrt{\left(\frac{\mathrm{L_t^2}}{6\left|x_0\right|}\right)^2+\mathrm{L_t^2}-\sigma\left(\frac{\mathrm{L_t^3}\sin\beta}{3\mu\left|x_0\right|\mathcal{A}}\right)}}{2} \\
M &= \mu\frac{G\mathrm{L_t}\mathcal{A}}{4} \\
&\quad \left\{\left[1+\left(\frac{2\lambda_x}{\mathrm{L_t}}\right)^2\right]\left(1+\frac{4x_0\lambda_x}{\mathrm{L_t^2}}\right)-\frac{16x_0\lambda_x}{\mathrm{L_t^2}}\right\} \\
F_{i/o} &= F_{fi}+\frac{1}{2}F_G\mp\frac{M}{\mathrm{B_t}}
\end{aligned} \tag{2}$$

where G is the gravity, α is the pitch angle, β is the roll angle, h_{g} is the height of the center of mass, f is the rolling resistance coefficient, x_0 is the longitudinal offset of the track pressure center, λ_x is the longitudinal offset of the instantaneous steering center, $\mu_{\max}$ is the steering resistance coefficient when the steering radius is $\mathrm{B_t}/2$.

$$\begin{aligned}
F_G &= G\sin\alpha \\
F_f &= fG\cos\alpha \\
F_N^{f/r} &= G(\frac{b\cos\alpha\mp h_{\mathrm{g}}\sin\alpha}{\mathrm{L_a}}) \\
F_N^{f_{l/r}} &= F_N^f(\cos\beta\pm\frac{2h_{\mathrm{g}}\sin\beta}{\mathrm{B_a}}) \\
F_x &= F_f+F_G \\
F_y^{fr} &= \sqrt{\psi F_N^{fr}-\frac{F_x}{4}}
\end{aligned} \tag{3}$$

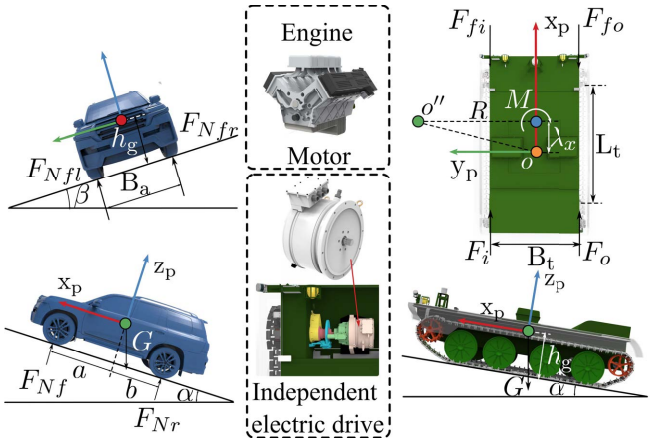

Fig. 2. Dynamic model and drive system

The drive system type of the skid-steering vehicle is a bilateral independent electric drive. For a skid-steering vehicle, part of the power provides longitudinal movement of the vehicle, and the other part provides lateral steering. The reserved power for the skid-steering vehicles is calculated as follows:

$$\begin{aligned}
T_{\mathrm{m}}^{i/o} &= \frac{F_{i/o}}{k_i k_{\mathrm{r}} r} \\
v^{i/o} &= \frac{4v_{\mathrm{px}}R\mp v_{\mathrm{px}}\mathrm{B_t}}{4R} \\
\omega_{\mathrm{m}}^{i/o} &= \frac{v_{\mathrm{px}}k_i k_{\mathrm{r}}}{r} \\
n_{\mathrm{m}}^{i/o} &= \frac{10800\omega_{\mathrm{m}}^{i/o}}{\pi} \\
P_{\mathrm{r}}^{i/o} &= P_{\max}(n_{\mathrm{m}}^{i/o})-\omega_{\mathrm{m}}^{i/o}T_{\mathrm{m}}^{i/o}
\end{aligned} \tag{4}$$

where $T_{\mathrm{m}}^{i/o}$ is the maximum output torque of the inner or outer drive motor, $v_{i/o}$ is the inner or outer track speed, $\omega_{\mathrm{m}}^{i/o}(\mathrm{rad/s})$ and $n_{\mathrm{m}}^{i/o}(\mathrm{rpm})$ is the speed of the inner or outer drive motor, k_i is the different gears of the transmission ratio, k_r reducer transmission ratio, $P_{\max}(n_{\mathrm{m}}^{i/o})$ is the maximum output power of the inner or outer motor at a specific speed, which can be obtained from the external characteristic curve.

For Ackermann steering vehicles, the engine output power is mainly used to provide longitudinal movement of the vehicle, and the factor limiting lateral steering is whether the lateral adhesion is sufficient. The reserved power and minimum turning radius for the Ackermann steering vehicle are calculated as follows:

$$\begin{aligned}
T_{\mathrm{e}} &= \frac{F_x}{k_i k_{\mathrm{r}} r} \\
\omega_{\mathrm{e}} &= \frac{v_{\mathrm{px}}k_i k_{\mathrm{r}}}{r} \\
n_{\mathrm{e}} &= \frac{10800\omega_{\mathrm{e}}}{\pi} \\
P_{\mathrm{r}} &= P_{\max}(n_{\mathrm{e}})-\omega_{\mathrm{e}}T_{\mathrm{e}} \\
R_{\min} &= \frac{mv_{\mathrm{px}}^2}{F_y^{fl}-G\sin\beta}
\end{aligned} \tag{5}$$

where v_{px} is the velocity of the vehicle, T_{e} is the maximum output torque of the engine, $\omega_{\mathrm{e}}(\mathrm{rad/s})$ and $n_{\mathrm{e}}(\mathrm{rpm})$ is the speed of the engine, k_i is the different gears of the transmission ratio, k_r reducer transmission ratio, $P_{\max}(n_{\mathrm{e}})$ is the maximum output power of engine at a specific speed, which can be obtained from the external characteristic.

By ensuring a certain threshold of reserved power and lateral adhesion, the curvature and the pose of the HDBP when passing through a specific terrain are limited as the control boundary for HDBP generation.

B. Extension And Selection of HDBP Library

The extension and selection of HDBP is defined as the following optimization problem, as is shown in Equation 6. The extension algorithm completes the splicing and transition of HDBP online, and the selection algorithm chooses the minimum time consumption sequence of HDBP to generate

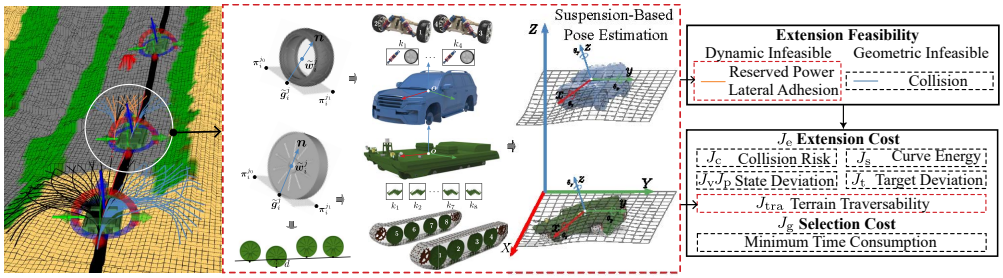

Fig. 3. Schematic diagram of HDBP extension and selection process

the spatiotemporal trajectory, as is shown in Fig. 3.

$$\begin{aligned} \min_{N} \quad & \sum_{k=0}^{N} J_{\mathrm{g}}(dbp_k) \\ s.t. \quad & \boldsymbol{s}_0 = \boldsymbol{s}_{\mathrm{start}}, \boldsymbol{s}_N = \boldsymbol{s}_{\mathrm{target}} + \boldsymbol{\varepsilon} \\ & J_{\mathrm{e}} = f_{\mathrm{e}}(\boldsymbol{s}_{\mathrm{target}}, \boldsymbol{\mathcal{M}}) \\ & mp_{k+1} = e(dbp_k, \boldsymbol{s}_k, J_{\mathrm{e}}) \\ & c(\boldsymbol{s}_k, dbp_k) \in \boldsymbol{E}_{\mathrm{pass}} \\ & r(\widetilde{dbp_k}) \in \boldsymbol{P}_{\mathrm{feasible}} \\ & \boldsymbol{P} = f_{\mathrm{t}}(\boldsymbol{s}_k, \boldsymbol{\mathcal{M}}) \\ & mp_k \in \boldsymbol{P} \end{aligned} \tag{6}$$

where J_{g} is the global cost function related to the time consumption of the whole trajectory, $\boldsymbol{s}$ is the state parameter at the primitive node (including position, course and velocity parameters), dbp is the extended HDBP, and $\boldsymbol{E}_{\mathrm{pass}}$ is the passable area, c is the function of collision check, P_{feasible} is the threshold of reserved power, r is the function of calculating the reserved power or lateral adhesion, f_{e} is the function of calculating the extension cost, e is the function of HDBP extension, J_{e} is the HDBP extension cost.

1) Terrain Traversablity Cost Based on Pose Estimation: In the process of extension of HDBP, it is necessary to guide the HDBPs to extend in relatively flat areas and ensure that the extended HDBPs are in dynamic constraints. Hence, both environment features and the suspension system of the vehicle are considered to estimate the poses of HDBPs to calculate the terrain traversability cost of HDBP J_{tra}, as is shown in Equation 7. In addition, the reserved power or lateral adhesion P_{r} is checked based on the estimated poses to determine whether the HDBP is dynamically feasible or not.

$$J_{\mathrm{tra}} = \sum_{n=2}^{N_{\mathrm{p}}} \frac{\dot{\alpha}_n + \dot{\beta}_n + \ddot{z}_n}{3} \tag{7}$$

where, N_{p} represent the number of nodes of HDBP.

The process of pose estimation is shown in Fig. 3. First, the two-dimensional grid patch $\boldsymbol{\Omega}_i^j$ of each wheel is calculated based on the HDBP node $\{\boldsymbol{s}_i = [x_i, y_i, \theta_i]^{\mathrm{T}} | \boldsymbol{s}_i \in \boldsymbol{S}\}$, $\boldsymbol{S}$ is the set of nodes of HDBP, as shown in Equation 8-10. And the three-dimensional coordinates set $\boldsymbol{\mathcal{P}}$ in the grid patch through the elevation map is obtained, as shown in Equation 11.

$$\boldsymbol{\mathcal{R}}_{\mathrm{p}}^{\mathrm{w}} = \begin{bmatrix} \cos\theta_i & \sin\theta_i \\ -\sin\theta_i & \cos\theta_i \end{bmatrix}, \boldsymbol{\mathcal{T}}_{\mathrm{p}}^{\mathrm{w}} = \begin{bmatrix} x_i \\ y_i \end{bmatrix} \tag{8}$$

$$\boldsymbol{\pi}_i^{j_{0/1}} = \begin{bmatrix} x_i^{j_{0/1}} \\ y_i^{j_{0/1}} \end{bmatrix} = \boldsymbol{\mathcal{R}}_{\mathrm{p}}^{\mathrm{w}} \begin{bmatrix} l_{oj} \pm \frac{l_{\mathrm{w}}}{2} \\ w_{oj} \pm \frac{w_{\mathrm{w}}}{2} \end{bmatrix} + \boldsymbol{\mathcal{T}}_{\mathrm{p}}^{\mathrm{w}} \tag{9}$$

$$\boldsymbol{\Omega}_i^j = \{x \in [x_i^{j_0}, x_i^{j_1}], y \in [y_i^{j_0}, y_i^{j_1}]\} \tag{10}$$

where $\boldsymbol{\mathcal{R}}_{\mathrm{p}}^{\mathrm{w}}$ and $\boldsymbol{\mathcal{T}}_{\mathrm{p}}^{\mathrm{w}}$ represent the rotation matrix and translation matrix of transformation between the vehicle coordinate and the world coordinate, i represents the index of HDBP node, j represents the index of the wheel, l_{oj} and w_{oj} represent the coordinate of the center of the wheel in vehicle coordinate, l_{w} and w_{w} represent length and width of the wheel.

$$\boldsymbol{\mathcal{P}} = \{\widetilde{\boldsymbol{s}}(x, y, z) | \boldsymbol{s} \in \boldsymbol{\Omega}_i^j\} \tag{11}$$

PCA method is used to calculate the three-dimensional coordinates of the center of each grid patch in the world coordinate $\widetilde{\boldsymbol{g}}_i^j$, normal vector $\boldsymbol{n}$ and suspension attachment points $\widetilde{\boldsymbol{w}}_i^j$, as shown in Equation 12-15. As for type I vehicle, in the same way, the three-dimensional center coordinates $\widetilde{\boldsymbol{q}}_i$ of the tracks on both sides for type I vehicle or the three-dimensional center coordinates of the vehicle for type II vehicle are calculated.

$$\widetilde{\boldsymbol{g}}_i^j = \frac{1}{k} \sum_{\widetilde{\boldsymbol{s}} \in \boldsymbol{\mathcal{P}}} \widetilde{\boldsymbol{s}} \tag{12}$$

$$\mathrm{cov} = \sum_{\widetilde{\boldsymbol{s}} \in \mathcal{P}} (\widetilde{\boldsymbol{s}} - \widetilde{\boldsymbol{g}}_i^j)(\widetilde{\boldsymbol{s}} - \widetilde{\boldsymbol{g}}_i^j)^{\mathrm{T}} \in \mathbb{R}^{3\times 3} \tag{13}$$

$$\boldsymbol{n} = \min(eig(\mathrm{cov})) \tag{14}$$

$$\widetilde{\boldsymbol{w}}_i^j = \widetilde{\boldsymbol{g}}_i^j + \frac{\boldsymbol{n} \cdot r}{\|\boldsymbol{n}\|} \tag{15}$$

where cov is the covariance matrix of the grid coordinate in the grid patch, eig is the set of eigenvalues of the matrix, k is the number of grids in the grid patch, r is the radius of the wheel.

According to the three-dimensional center coordinates of each wheel and the coordinates of the track for type II vehicle or the rough coordinates of the vehicle, the wheel ground contact matrix $\boldsymbol{C}$ is obtained, as is shown in Equation 16.

$$c_i^j = 0.5 - 0.5\mathrm{sgn}(|\widetilde{\boldsymbol{q}}_i.z - \widetilde{\boldsymbol{w}}_i^j.z| - d), \forall j \in \{1, 2, ..., N_l\} \tag{16}$$

where d represents the maximum stroke of suspension deformation, sgn is the sign function.

$$\boldsymbol{C} = \begin{bmatrix} c_i^1 & 0 & \cdots & 0 \\ 0 & c_i^2 & \cdots & 0 \\ \vdots & \vdots & & \\ 0 & 0 & \cdots & c_i^N \end{bmatrix} \in \mathbb{R}^{N\times N} \tag{17}$$

where $\boldsymbol{C}$ is a reversible real symmetric matrix.

When estimating pose, it is assumed that the vehicle is in a static equilibrium state. Equation 18 is used to estimate the pose $\boldsymbol{\Theta}_i = [z_{oi}, \alpha_i, \beta_i]^{\mathrm{T}} \in \mathbb{R}^{3\times 1}$ of vehicle. where, $\Delta z_i^j = z_{oi} + l_o^j\alpha_i + w_o^j\beta_i - z_i^j$, z_{oi}, α_i, β_i represent vertical coordinates, pitch angle, roll angle of the vehicle. The Equation 18 can be expressed as a standard state transition matrix equation, as is shown in Equation 19.

$$\begin{cases} \sum\limits_{j=0}^{N} k^j c_i^j \Delta z_i^j - mg = 0 \\ \sum\limits_{j=0}^{N} k^j c_i^j \Delta z_i^j |l_o^j| = 0 \\ \sum\limits_{j=0}^{N} k^j c_i^j \Delta z_i^j |w_o^j| = 0 \end{cases} \tag{18}$$

$$\boldsymbol{K}\boldsymbol{C}_i\boldsymbol{A}\boldsymbol{\Theta}_i - \boldsymbol{K}\boldsymbol{C}_i\boldsymbol{Z}_i^j + \boldsymbol{B} = \boldsymbol{0} \tag{19}$$

where $\boldsymbol{K} = \begin{bmatrix} k^1 & 0 & \cdots & 0 \\ 0 & k^2 & \cdots & 0 \\ \vdots & \vdots & \cdots & 0 \\ 0 & 0 & \cdots & k^N \end{bmatrix} \in \mathbb{R}^{N\times N}$,

$\boldsymbol{A} = \begin{bmatrix} 1 & l_o^1 & w_o^1 \\ 1 & l_o^2 & w_o^2 \\ \vdots & \vdots & \vdots \\ 1 & l_o^N & w_o^N \end{bmatrix} \in \mathbb{R}^{N\times 3}$,

$\boldsymbol{B} = \begin{bmatrix} -mg \\ -mg \\ \vdots \\ -mg \end{bmatrix} \in \mathbb{R}^{N\times 3}$, $\boldsymbol{Z} = \begin{bmatrix} z_i^1 \\ z_i^2 \\ \vdots \\ z_i^8 \end{bmatrix} \in \mathbb{R}^{N\times 1}$. Let $\boldsymbol{M}_i = \boldsymbol{K}\boldsymbol{C}_i\boldsymbol{A} \in \mathbb{R}^{N\times 3}$, $\boldsymbol{N}_i = -\boldsymbol{K}\boldsymbol{C}_i\boldsymbol{Z}_i + \boldsymbol{B} \in \mathbb{R}^{N\times 1}$. The simplified form of Equation 19 is shown in Equation 20. The final three-dimensional pose estimation of the vehicle is shown in Equation 21.

$$\boldsymbol{M}_i\boldsymbol{\Theta}_i - \boldsymbol{N}_i = \boldsymbol{0} \tag{20}$$

$$\boldsymbol{\Theta}_i = \boldsymbol{M}_i^{-1}\boldsymbol{N}_i \tag{21}$$

2) Extension Cost: The extension cost function J_{e} is given by Equation 22, where $p_m, J_{\mathrm{p}}, J_{\mathrm{v}}, J_{\mathrm{s}}, J_{\mathrm{c}}, J_{\mathrm{t}}$ is defined in the previous work [18].

$$J_{\mathrm{e}} = p_m(\omega_{\mathrm{p}}J_{\mathrm{p}} + \omega_{\mathrm{v}}J_{\mathrm{v}} + \omega_{\mathrm{s}}J_{\mathrm{s}} + \omega_{\mathrm{c}}J_{\mathrm{c}} + \omega_{\mathrm{t}}J_{\mathrm{t}} + \omega_{\mathrm{tra}}J_{\mathrm{tra}}) \tag{22}$$

where $\omega_{\mathrm{p}}, \omega_{\mathrm{v}}, \omega_{\mathrm{s}}, \omega_{\mathrm{c}}, \omega_{\mathrm{t}}, \omega_{\mathrm{tra}}$ are the weight coefficients of the corresponding cost value, which adjust the different costs to the same order of magnitude.

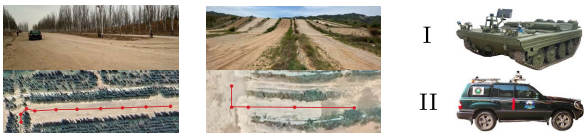

(a) Scene 1 (b) Scene 2 (c) Vehicle

Fig. 4. Test condition

III. EXPERIMENTAL RESULTS AND DISCUSSION

This paper first demonstrates the characteristics of HDBPs that consider terrain semantic surfaces, such as soft soil roads, and terrain geometric roughness, such as slope, and then uses the generated HDBP library to test the algorithm in real scenes using heterogeneous vehicles, as shown in Fig. 4. The structural and actuator parameters of the vehicles are shown in Table I, where type I vehicle represent skid steering vehicle, type II vehicle represent Ackermann steering vehicle, W and L are the width and length of the vehicle body, $\delta_{\max}$ and $\Delta v_{\max}$ are the limit values of the lateral control variables of heterogeneous vehicle.

TABLE I

VEHICLE GEOMETRIC PARAMETERS AND ACTUATOR CONSTRAINTS.

Type	W (m)	L (m)	m (kg)	$\delta_{\max}$ (rad)	$\Delta v_{\max}$ (m/s)
I	3.3	5.2	8960	-	5.3
II	1.9	4.3	1700	$\pi/6$	-

A. HDBP Library

In this section, the HDBPs on flat hard roads, soft soil roads, and slope roads are displayed and compared.

1) HDBP Library Result: The situation of HDBP library related to environment terrain is shown in Table II, where Terrain represents the terrain feature, $\bar{v}_m$ is set to 1m/s for demonstration, mainly because it has rich behavior performance for different terrain feature at low speeds, N_m is the number of the primitives in the corresponding velocity range. N_m is not only related to extracted driving behavior but also related to the terrain semantic surface and terrain geometric roughness. $\overline{k}$ is the average proportion of straight line segments, $\overline{l}$ is the average length. Fig. 5 shows the power consumption(I) and adhesion requirements(II) of HDBP on different terrains, heading angle deviations and lateral position deviations.

TABLE II

HDBP LIBRARY RELATED TO TERRAIN.

Type	Terrain	$\bar{v}_m$ (m/s)	N_m	$\overline{k}$	$\overline{l}$(m)
I	flat	1	46	0.1164	15
I	soft	1	15	0.5325	8
I	slope(10)	1	13	0.2491	15
I	slope(20)	1	3	0.4194	15
II	flat	1	46	0.1069	18
II	soft	1	45	0.1069	18
II	slope(10)	1	45	0.1069	18
II	slope(20)	1	17	0.1772	18

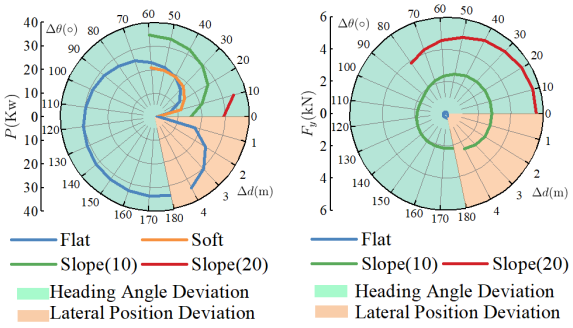

(a) I-Power Consumption (b) II-Adhesion Requirement

Fig. 5. Comparison of HDBP in different terrains

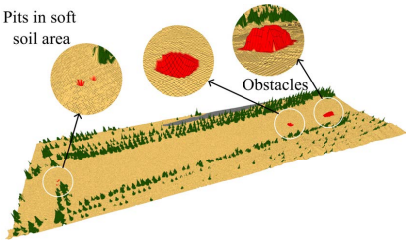

Fig. 6. Scene 1 terrain features

2) HDBP Library Discussion: It can be observed from Table II that The number of HDBP of I vehicle is 28.89% and 17.65% of the number of HDBP of II vehicle when the slope is 10 degrees and 20 degrees. Limited by the external characteristics of the drive components and the mass of the vehicle, the steering ability of I vehicle on slopes is weaker than that of II vehicle. The number of HDBP of I vehicle on soft roads is 33.33% of the number of HDBP of II vehicle. Besides, the length of the HDBP of I vehicle is also shorter than that of II vehicle. This is because the continuous steering of the I vehicle on soft roads will cause great bulldozing resistance due to its steering characteristics. Therefore, the driving behavior of I vehicle on soft roads adopts alternating straight driving and small steering to avoid bulldozing resistance. Because of the limitation of the ground adhesion on soft soil roads, II vehicle only has low-speed behavior with limited curvature and acceleration.

It can be observed from Fig. 5 that as terrain traversability cost increases, the power consumption of I vehicle and the lateral adhesion requirement of II vehicle increase. The power consumption and the lateral adhesion requirement are limited by the power characteristics of the drive components and the upper limit of the adhesion provided by the ground. Therefore, the steering capabilities of both vehicles have declined, so that the number of HDBP for both vehicles in higher terrain traversability cost scenes is smaller. In addition, the proportion of straight-line segments of HDBP is larger in those scenes, as shown in Table II.

B. Motion Planning

The motion planning experiments for heterogeneous vehicles were conducted in two typical scenes, as shown in Fig. 6 and Fig. 11. Scene 1 includes a soft soil area, a flat hard dirt area, and two pits which may cause contact free for the II vehicle. Scene 2 includes obstacles in the slope area.

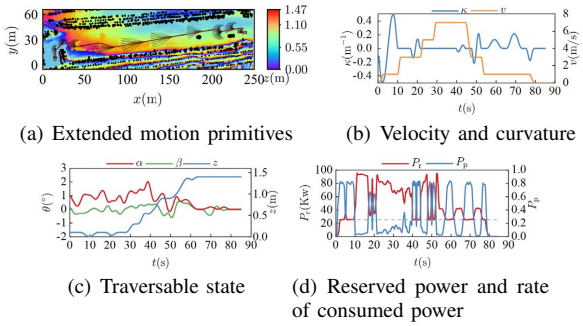

(a) Extended motion primitives (b) Velocity and curvature

(c) Traversable state (d) Reserved power and rate of consumed power

Fig. 7. I-HDBP

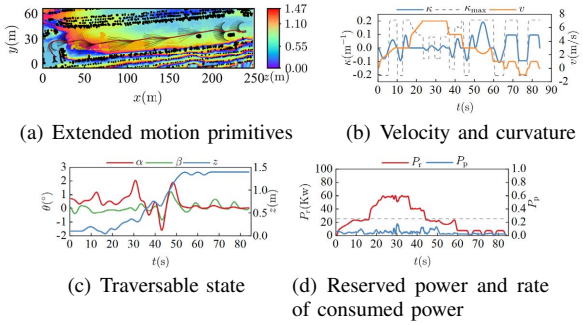

(a) Extended motion primitives (b) Velocity and curvature

(c) Traversable state (d) Reserved power and rate of consumed power

Fig. 8. II-HDBP

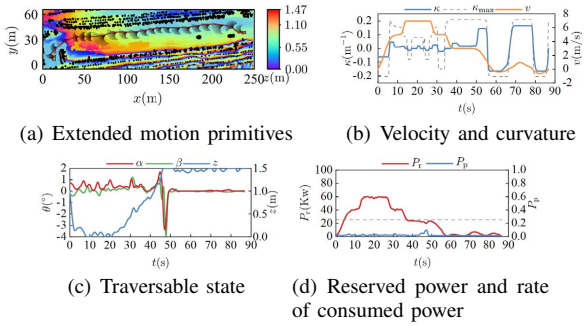

(a) Extended motion primitives (b) Velocity and curvature

(c) Traversable state (d) Reserved power and rate of consumed power

Fig. 9. THA*

1) Motion Planning Result: For scenes 1 and 2, the DBP-based motion planning results, THA* [5] results, OBTPAP [19] are shown in Fig. 7 - Fig. 10 and Fig. 13 - Fig. 15, the arrows indicate the poses of the start (orange) and target (red) pose.

2) Motion Planning Discussion: It can be observed from Fig. 7(a) - Fig.12(a) that due to its lateral and longitudinal coupling characteristics and power limitations, I vehicle uses large steering to avoid obstacles at low velocity and maintains straight-line motion at high velocity. However, II vehicle uses small steering to adjust their pose at high velocity. II vehicle has more velocity adjustment behavior, but I vehicle often steers at a fixed velocity, as is shown in

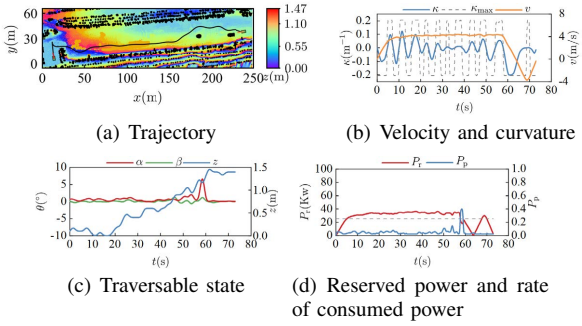

(a) Trajectory (b) Velocity and curvature

(c) Traversable state (d) Reserved power and rate of consumed power

Fig. 10. OBTPAP

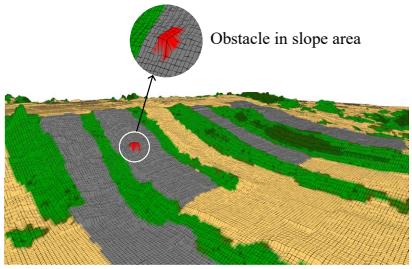

Fig. 11. Scene 2 terrain features

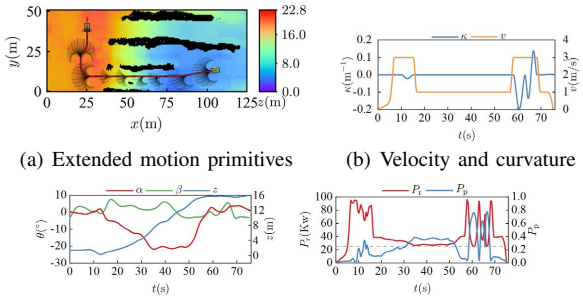

(a) Extended motion primitives (b) Velocity and curvature

(c) Traversable state (d) Reserved power and rate of consumed power

Fig. 12. I-HDBP

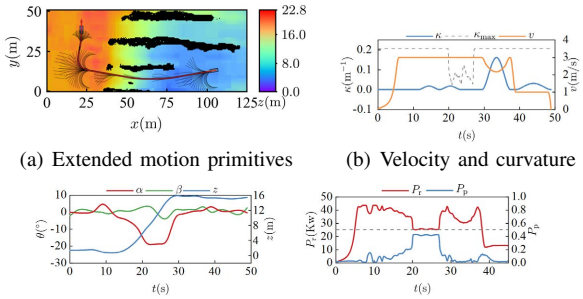

(a) Extended motion primitives (b) Velocity and curvature

(c) Traversable state (d) Reserved power and rate of consumed power

Fig. 13. II-HDBP

Fig. 7(b) and Fig. 8(b). Regarding the two pits, due to the influence of the suspension system and ground contact of the I vehicle, I vehicle directly passed through the pits, while the II vehicle chooses to go around in order to avoid contact free. On the soft road, as shown in Fig. 7(a) and Fig. 8(a), I vehicle uses alternating straight and steering behaviors, which effectively reduce the bulldozing resistance in the soft road. II vehicle decelerates in advance for the soft road to reduce the slip effect, which improves the feasibility of the trajectory.

It can be observed from Fig. 7(a), Fig. 8(a), Fig. 9(a) that the HDBP based method can reach the target pose by extending only 12 layers and 10 layers HDBP respectively, while THA* needs 21 layers. The reason is the rich HDBP library, which improves the efficiency of the planning algorithm. As is shown in Fig. 10(a), the OBTPAP method has a gear switch behavior on soft road, causing large lateral and longitudinal accelerations, and the feasibility of the trajectory is greatly reduced. For the two pits near the target pose, THA* and OBTPAP do not use the pose estimation method based on the ground contact, causing a sudden change in the pitch and roll angles of the vehicle, as shown in Fig. 9(c) and Fig. 10(c), which will lead to irreversible damage to the vehicle. Since the comparison algorithm does not consider the traversability of the environment, the proposed algorithm is better than the comparison algorithm in terms of the average traversability value and the entire traversability distribution, as is shown in Fig. 16(a). Due to the influence of the pit, the maximum traversability cost of the comparison algorithm is larger.

As is shown in Fig. 12(a) and Fig. 13(a), based on the HDBP of the slope and the reserved power check, I vehicle aligns the gradient direction of the slope before entering the slope to avoid steer on the slope. However, the II vehicle still has weak steering ability, so it uses small-angle steering to avoid obstacles on the slope. In addition, it can be observed from Fig. 12(b) and Fig. 12(d) that due to the external characteristics of the drive components of the I vehicle, the velocity is reduced when going uphill to ensure sufficient reserved power to resist interference from environmental uncertainties.

As is shown in Fig. 14(a) and Fig. 15(a), THA* and OBTPAP still steer when going uphill. Both methods exceed the limit of the turning radius at the red circle, resulting in infeasiblility of the generated trajectory, as is shown in Fig. 14(b) and Fig. 15(b). Besides, OBTPAP still has a large velocity adjustment on the slope. So, more drive power and ground adhesion are required which can easily lead to an unfeasible path. Fig. 16(b) is the traversable cost distribution diagram of each algorithm, the wider the diagram, the higher the frequency of the cost. Due to the steering on the slope, the pitch angle and roll angle of the comparison algorithm change greatly on the slope, which also makes the traversability of the comparison algorithm greater than the proposed method.

IV. CONCLUSIONS

This paper proposes a heterogeneous vehicle motion planning method based on HDBP generation, extension, and selection that considers vehicle characteristics and terrain features in the off-road scene. The primitive optimization

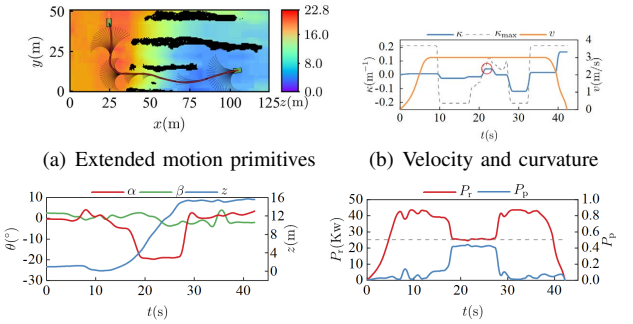

(a) Extended motion primitives (b) Velocity and curvature

(c) Traversable state (d) Reserved power and rate of consumed power

Fig. 14. THA*

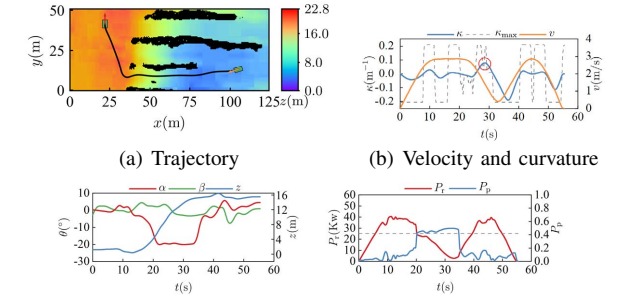

(a) Trajectory (b) Velocity and curvature

(c) Traversable state (d) Reserved power and rate of consumed power

Fig. 15. OBTPAP

method proposed in this paper, by setting constraints on the driving behavior of heterogeneous vehicles in different terrains and constraints on the differentiated characteristics of vehicles in multiple dimensions, effectively improves the matching degree of primitives for different off-road scenes and vehicle types. By fusing a multi-point contact model with suspension system characteristics for pose estimation, followed by reserved power and ground adhesion limits to constrain vehicle behavior in off-road scenes, the HDBP extension and selection method proposed in this paper effectively reduces the terrain traversability cost for heterogeneous vehicles. Founded on the above improvements, the method proposed in this paper enhances the accessibility of heterogeneous vehicles in off-road scenes, and the HDBP-based planning results highlight the advantages of the respective characteristics of heterogeneous vehicles.

In the future, we will realize the deep integration of the planning methods proposed in this paper and the model-based motion control methods to improve the overall performance of unmanned driving of heterogeneous vehicles.

REFERENCES

[1] Xu, Long, et al. "An Efficient Trajectory Planner for Car-Like Robots on Uneven Terrain." 2023 IEEE/RSJ International Conference on Intelligent Robots and Systems (IROS). IEEE, 2023.

[2] Fukuda, Yukiya, et al. "Dense Traversability Estimation System for Extreme Environments." 2023 IEEE Intelligent Vehicles Symposium (IV). IEEE, 2023.

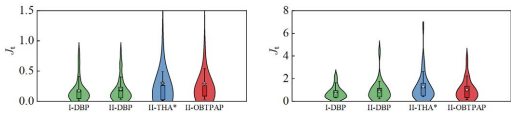

(a) Scene 1 (b) Scene 2

Fig. 16. Comparison of traversable cost

[3] Krüsi, Philipp, et al. "Driving on point clouds: Motion planning, trajectory optimization, and terrain assessment in generic nonplanar environments." Journal of Field Robotics 34.5 (2017): 940-984.

[4] Klančar, Gregor, and Sašo Blažič. "Optimal constant acceleration motion primitives." IEEE Transactions on Vehicular Technology 68.9 (2019): 8502-8511.

[5] Thoresen, Marius, et al. "Path planning for UGVs based on traversability hybrid A." IEEE Robotics and Automation Letters 6.2 (2021): 1216-1223.

[6] Ding, Wenchao, et al. "Safe trajectory generation for complex urban environments using spatio-temporal semantic corridor." IEEE Robotics and Automation Letters 4.3 (2019): 2997-3004.

[7] Bergman, Kristoffer, Oskar Ljungqvist, and Daniel Axehill. "Improved optimization of motion primitives for motion planning in state lattices." 2019 IEEE Intelligent Vehicles Symposium (IV). IEEE, 2019.

[8] Edmonds, Mark, et al. "A tale of two explanations: Enhancing human trust by explaining robot behavior." Science Robotics 4.37 (2019): eaay4663.

[9] Li, Guofa, et al. "Extraction of descriptive driving patterns from driving data using unsupervised algorithms." Mechanical Systems and Signal Processing 156 (2021): 107589.

[10] Waibel, Gabriel Günter, et al. "How rough is the path? Terrain traversability estimation for local and global path planning." IEEE Transactions on Intelligent Transportation Systems 23.9 (2022): 16462-16473.

[11] Atas, Fetullah, Grzegorz Cielniak, and Lars Grimstad. "Elevation State-Space: Surfel-Based Navigation in Uneven Environments for Mobile Robots." 2022 IEEE/RSJ International Conference on Intelligent Robots and Systems (IROS). IEEE, 2022.

[12] Gasparino, Mateus V., et al. "Wayfast: Navigation with predictive traversability in the field." IEEE Robotics and Automation Letters 7.4 (2022): 10651-10658.

[13] J. Wang et al., "Towards Efficient Trajectory Generation for Ground Robots beyond 2D Environment," 2023 IEEE International Conference on Robotics and Automation (ICRA), London, United Kingdom, 2023, pp. 7858-7864, doi: 10.1109/ICRA48891.2023.10160330 .

[14] Zhang, Kai, et al. "Traversability assessment and trajectory planning of unmanned ground vehicles with suspension systems on rough terrain." Sensors 19.20 (2019): 4372.

[15] Sharma, Lakshay, et al. "RAMP: A Risk-Aware Mapping and Planning Pipeline for Fast Off-Road Ground Robot Navigation." 2023 IEEE International Conference on Robotics and Automation (ICRA). IEEE, 2023.

[16] Guo, Yuqing, et al. "Trajectory planning for an autonomous vehicle in spatially constrained environments." IEEE Transactions on Intelligent Transportation Systems 23.10 (2022): 18326-18336.

[17] B. Wang, J. Gong, and H. Chen, "Motion primitives representation, extraction and connection for automated vehicle motion planning applications," IEEE Trans. Intell. Transp. Syst., vol. 21, no. 9, pp. 3931–3945, Sep. 2020.

[18] H. Guan, B. Wang, J. Gong and H. Chen, "Coordinated Motion Planning for Heterogeneous Autonomous Vehicles Based on Driving Behavior Primitives," in IEEE Transactions on Intelligent Transportation Systems, vol. 24, no. 11, pp. 11934-11949, Nov. 2023.

[19] Li, Bai, et al. "Optimization-based trajectory planning for autonomous parking with irregularly placed obstacles: A lightweight iterative framework." IEEE Transactions on Intelligent Transportation Systems 23.8 (2021): 11970-11981.